NJC

PAPER

View Article Online
View Journal | View Issue

Cite this: *New J. Chem.*, 2019, 43, 16981

Ti functionalized hierarchical-pore UiO-66(Zr/Ti) catalyst for the transesterification of phenyl acetate and dimethyl carbonate†

Bingying Jia, [ab] Miaojiang Wu, [ab] Hua Zhang, [a] Yi Zeng [a] and Gongying Wang *[a]

Received 15th August 2019,
Accepted 8th October 2019

DOI: 10.1039/c9nj04241e

rsc.li/njc

Titanates are frequently used as precursors to prepare transesterification catalysts with Ti^{IV} species. Unfortunately, it is challenging to control the dispersity of Ti^{IV} active sites on supports. Herein, a series of Ti^{IV} species is anchored on abundant linker vacancy sites by introducing point and large scale defects in UiO-66(Zr/Ti) with hierarchical-pore structure. The catalyst functionalized by titanium(IV) oxide bis(2,4-pentanedionate) shows excellent catalytic performance in the transesterification of dimethyl carbonate with phenyl acetate. The catalysts are characterized by XRD, FT-IR, N_2 adsorption–desorption, XPS, SEM and STEM-HAADF techniques. The results demonstrate that the delicate mesopores in the support can not only exhibit a large surface area for the distribution of the active sites, but also provide better mass transfer performance. Meanwhile, the introduction of octahedral Ti^{IV} ions raises the activity of the catalyst *via* more coordinatively unsaturated Zr^{IV} sites. Furthermore, using titanium(IV) oxide bis(2,4-pentanedionate) as a Ti source can effectively prevent the condensation of tetrahedral Ti^{IV} species anchored on the hierarchical-pore UiO-66(Zr/Ti) support.

Introduction

Diphenyl carbonate (DPC) has been widely applied as a green carbonyl source for various carbonylation reactions.[1–3] As a highly reactive reagent, it can be conveniently used for the non-phosgene preparation of polycarbonates (PCs) by a melt polymerization process.[4] Several methods including oxidative carbonylation of phenol (PhOH), and transesterification of dimethyl carbonate (DMC) and PhOH or phenyl acetate (PA) have been applied to synthesize DPC.[5–10] Among them, the transesterification of DMC and PA is regarded as one of the most suitable synthesis routes for commercial production of DPC due to the large equilibrium constant and atom-economy.

Generally, heterogeneous catalysts with Ti^{IV} species have been developed to produce DPC through transesterification.[11–14] To date, the reported heterogeneous catalysts are mainly derived from depositing TiO_2 on supports including metal oxide, SiO_2 and carbon.[11,15,16] However, these traditional inert carriers are unfavourable to achieve the uniform dispersion of the Ti^{IV} species, because it is quite difficult to locate and control the types and distributions of hydroxyl groups on their surface. To our knowledge, the uniform distribution of Ti^{IV} species on catalyst supports is difficult, mainly due to the extremely high reactivity of the titanium dioxide precursors.[17] Organo-titanium, for example, $Ti(OR)_4$, tends to hydrolyze quickly and form dense precipitates containing $Ti(OR)_{4-x}(OH)_x$ species and corresponding oligomers.[18] The emerging dense precipitates lead to partial blocking of the pores in catalyst supports and result in the reduction of Ti atom utilization. Consequently, the key issues in the synthesis of heterogeneous catalysts containing Ti^{IV} species is how to effectively prevent the aggregation of Ti^{IV} active sites by developing a suitable Ti source and supports.

Numerous studies have been conducted concentrating upon the construction and modification of Zr-based catalyst supports and their application in transesterification processes.[19–22] Especially, UiO-66(Zr) has attracted particular interest due to its remarkable thermal and chemical stability and superior catalytic activity based on the Lewis acid sites derived from introducing missing-linker and missing-cluster defects.[23–25] In general, the surface defects, internal imperfections, and the interaction with metal and support are in favor of enhancing the catalytic activity of UiO-66(Zr).[26] UiO-66(Zr) consists of hexanuclear clusters in which each Zr^{IV} ion is connected to linear 1,4-benzenedicarboxylate (BDC) ligands. Kim *et al.*[27] reported that Ti^{IV} ions could be incorporated into the node of

[a] *Chengdu Institute of Organic Chemistry, Chinese Academy of Sciences, Chengdu 610041, China. E-mail: wanggongying1102@126.com*
[b] *National Engineering Laboratory for VOCs Pollution Control Material & Technology, University of Chinese Academy of Sciences, Beijing 101408, China*

† Electronic supplementary information (ESI) available. See DOI: 10.1039/c9nj04241e

UiO-66(Zr) by exchanging with partial Zr^{IV} ions. Nguyen *et al.*[28] and Santaclara *et al.*[29] found that Ti^{IV} ions could also be conjectured to occupy the missing-linker sites of UiO-66(Zr). The modification of the electronic situation at linker and/or metal node vacancies could significantly affect the reactive properties of the catalyst.[26,30,31] Vermoortele *et al.*[31] demonstrated that the excellent catalytic activity of UiO-66(Zr) can be ascribed to the coordinatively unsaturated Zr^{IV} sites, acting as Lewis acid sites, rather than a modified Lewis acid strength. Moreover, it was proved that a large number of missing-linker defects could improve the specific surface area and expose more Lewis acid sites for UiO-66(Zr).[30] However, the pure microporous structure of UIO-66(Zr) might restrict the accessibility of bulky molecules within it. Therefore, the development of hierarchical-pore UiO-66(Zr) containing both micropores and mesopores is of great significance. In the interconnected network structure of UiO-66(Zr), micropores are beneficial to maintaining the functionality of the catalyst support, while the presence of mesopores can bring a positive impact on the molecular diffusion.[32]

In this work, the catalysts derived from Ti functionalized hierarchical-pore UiO-66(Zr/Ti) (H-UiO-66(Zr/Ti)) were prepared. The starting H-UiO-66(Zr) sample was synthesized by using an *in situ* self-assembly template strategy. Ti^{IV} ions were then incorporated in the node and at hydroxyl sites of the H-UiO-66(Zr) framework by ion-exchange. Furthermore, different Ti^{IV} species were grafted on supports for preparing Ti functionalized H-UiO-66(Zr/Ti) catalysts. The catalysts were used for the transesterification of DMC and PA, and the reaction conditions were investigated. The as-prepared Ti functionalized H-UiO-66(Zr/Ti) catalysts in this work exhibit high activity and small consumption, resulting from the appropriate distribution and state of Ti^{IV} ions, better mass transfer and a considerable density of structural defects of the support. Furthermore, H-UiO-66(Zr/Ti) as a catalyst support shows catalytic activity to a certain extent in this transesterification reaction. The aims of this work are described as follows: (1) the possibility of the preparation of the H-UiO-66(Zr/Ti) sample with abundant point and mesopore defects was explored by the incorporation of Ti^{IV} ions into H-UiO-66(Zr). (2) Investigating the effect of Ti sources on the distribution and state of Ti^{IV} active sites in order to prevent the condensation of Ti^{IV} species in the Ti functionalized catalysts. (3) The impact of different Ti^{IV} coordination environments on the activity of the transesterification catalysts was evaluated.

Experimental

Materials

Zirconium tetrachloride ($ZrCl_4$, 98%) and Titanium(IV) oxide bis(2,4-pentanedionate) ($TiO(acac)_2$, 98%) were purchased from Shanghai Macklin Biochemical Co. Ltd. Zinc nitrate hexahydrate ($Zn(NO_3)_2{\cdot}6H_2O$, 99%), 2-methylimidazole (98%), *N*,*N*′-dimethylformamide (DMF, 99.5%), and benzoic acid (HBC, 99%) were purchased from Chengdu Chron Chemical Co. Ltd. Terephthalic acid (TPA, 99%), titanocene dichloride ($TiCp_2Cl_2$, 98%) and

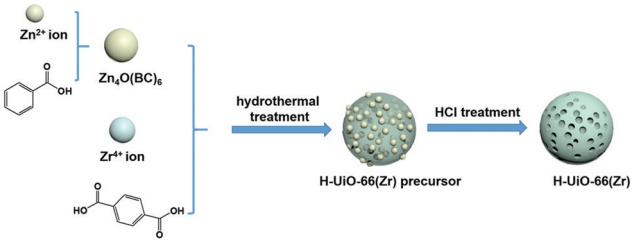

Scheme 1 Schematic representation for the preparation of H-UiO-66(Zr).

tetrabutyl titanate ($Ti(OBu)_4$, 98%) were purchased from Aladdin chemistry Co. Ltd. TS-1 was purchased from XFNANO Materials Tech Co. Ltd. All the reagents and solvents were used as received without further purification. Titanium-Citrate was self-made and the ORTEP structure is shown in Scheme S1 (ESI†).

Preparation of hierarchical-pore UiO-66 (H-UiO-66)

The synthesis of H-UiO-66 was achieved as per the reported method with some modifications (Scheme 1).[33] $Zn(NO_3)_2{\cdot}6H_2O$ (0.592 g, 2 mmol), HBC (7.320 g, 60 mmol), $ZrCl_4$ (0.480 g, 2 mmol), and TPA (0.664 g, 4.0 mmol) were dissolved in 80 mL of DMF. The obtained suspension was sonicated for 20 minutes and then transferred into a 100 mL autoclave in a preheated oven at 120 °C for 24 hours. After cooling to room temperature, the white product was centrifugated, washed several times with a mixture of DMF and methanol, and dried at 100 °C for 12 h. Then, the H-UiO-66(Zr) precursor was dispersed in HCl solution (pH = 1.0) and stirred for about 2 h to dissolve the acid-sensitive metal–organic assembling template ($Zn_4O(BC)_6$) and obtain the hierarchical-pore structure. The product was separated by centrifugation and washed with DMF and methanol several times. Finally, the H-UiO-66(Zr) support was dried at 100 °C overnight.

Preparation of mixed-metal H-UiO-66(Zr/Ti)

H-UiO-66(Zr/Ti) was prepared following a modification of a previously reported procedure (Scheme 2, Step 1).[27,34] Generally, 0.75 g of $TiCp_2Cl_2$ (3 mmol) was added into 60 mL of *N*,*N*-dimethylformamide (DMF), and the mixture was treated by ultrasonic wave for 40 minutes. Then, 0.8 g of the prepared H-UiO-66(Zr) was introduced into it and the suspension was transferred to a 100 mL autoclave, which was heated for 5 d at 85 °C. After cooling, the solid was obtained by filtration and washed with a mixture of DMF and methanol several times. The solid was left to soak in methanol for 2 days to remove the Ti^{IV} species adsorbed

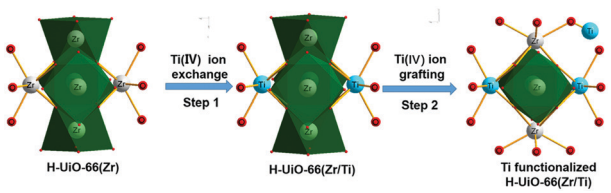

Scheme 2 Schematic representation for the preparation of Ti functionalized H-UiO-66(Zr/Ti).

on the surface. Finally, the desired product was centrifuged and dried at 100 °C overnight.

Preparation of Ti functionalized H-UiO-66(Zr/Ti)

Ti functionalized H-UiO-66(Zr/Ti) with different Ti sources was synthesized using the reported method; a slight modification was made to achieve a better effect (Scheme 2, Step 2).[35] $TiO(acac)_2$, $TiCp_2Cl_2$, $Ti(OBu)_4$ and Ti-Citrate were selected as Ti sources, respectively, for $TiO(acac)_2$-H-UiO-66(Zr/Ti) with a Ti : H-UiO-66(Zr/Ti) weight molar ratio of 0.2 : 1 (denoted 20% $TiO(acac)_2$-H-UiO-66(Zr/Ti)). 0.9 g of $TiO(acac)_2$ was dissolved in a mixture of 150 mL of methanol and 1 mL of deionized water. Then, this solution was mixed with 0.8 g of H-UiO-66(Zr/Ti) in a 250 mL flask. The suspension was heated to reflux at 65 °C in an oil bath for 12 h. After cooling, the powder was obtained through centrifugation and immersed in methanol (100 mL) for 12 h to remove unreacted metal ions. The mixture was centrifuged and dried to get the 20%$TiO(acac)_2$-H-UiO-66(Zr/Ti) sample. For comparison, 20%$TiO(acac)_2$-TS-1 was prepared using a similar method.

Characterization

X-ray diffraction (XRD) patterns were recorded using a Rigaku X-ray diffractometer with monochromatic Cu Kα in a scan range of 4° to 51°. N_2 adsorption–desorption isotherms were determined by using an ASAP 2460 at 77 K. Before adsorption measurements, the samples were degassed under vacuum at 120 °C for 5 h. The surface area was estimated by the Brunauer–Emmett–Teller (BET) equation, and micropore and mesopore size distributions were calculated using the H–K and Barrett–Joyner–Halanda (BJH) methods, respectively. Fourier transform infrared (FT-IR) spectroscopy was performed using a Nicolet-6700 instrument with samples prepared as KBr pellets at wavenumbers ranging from 4000 to 450 cm^{-1}. X-ray photoelectron spectroscopy (XPS) spectra were recorded using an Escalab 250Xi instrument with monochromatic Al Kα radiation. The morphological properties of the samples were imaged by using a JEOL JEM-5410LV scanning electron microscope (SEM) operated at 20 kV. The high-angle annular dark-field scanning transmission electron microscopy (HAADF-STEM) images and energy dispersive X-ray spectroscopy (EDX) mappings were generated using an FEI Tecnai G2 F20 transmission electron microscope equipped with an energy-dispersive X-ray spectrometer system and a high-angle angular dark-field detector was used at 200 kV. Thermogravimetric analysis (TGA) was performed using a TGA Q500 V20.10 Build 36 instrument with heating at 10 °C min^{-1} in a N_2 atmosphere.

Activity evaluation of the catalysts

The transesterification reaction of DMC (40 g, 0.44 mol) and PA (30 g, 0.22 mol) was carried out in a 100 mL three-neck glass flask. Additionally, the apparatus consisted of a magnetic stirring bar, a dropping funnel, a thermometer and a fractionating column. A mixture of 30 g of PA and 0.6 g of catalyst was charged into the flask. When the reaction mixture reached a temperature of 180 °C, DMC was dropwise added into it, and the reaction was conducted at 170–190 °C for a prescribed time. During the reaction, the unreacted DMC and the generation of methyl acetate, as the light components, were collected in a receiver flask. After completion of the reaction, the reaction products were obtained by centrifugation and determined by GC-MS using a HP-6890/5973 system. Moreover, the products were quantitatively analysed using an Agilent Technologies 7820 A gas chromatograph equipped with a DB-35 capillary column (30 m × 320 μm × 0.25 μm) and a flame ionization detector (FID).

Results and discussion

Catalyst characterization

Fig. 1(a) presents the XRD patterns of the Ti functionalized H-UiO-66(Zr/Ti) catalysts. All of the Ti functionalized samples show XRD patterns similar to that of pure H-UiO-66(Zr), indicating that the structure of the H-UiO-66(Zr) framework is retained. However, for Ti^{IV} ion exchanged samples, the most intense peak observed at around 7.3° shifts to a higher value (Fig. S1, ESI†). The phenomenon is a consequence of the shrinking of the crystal lattice due to the smaller radius of Ti^{IV} compared to that of Zr^{IV},[36,37] which indicates that some Ti^{IV} species are exchanged rather than grafted on linker vacancy

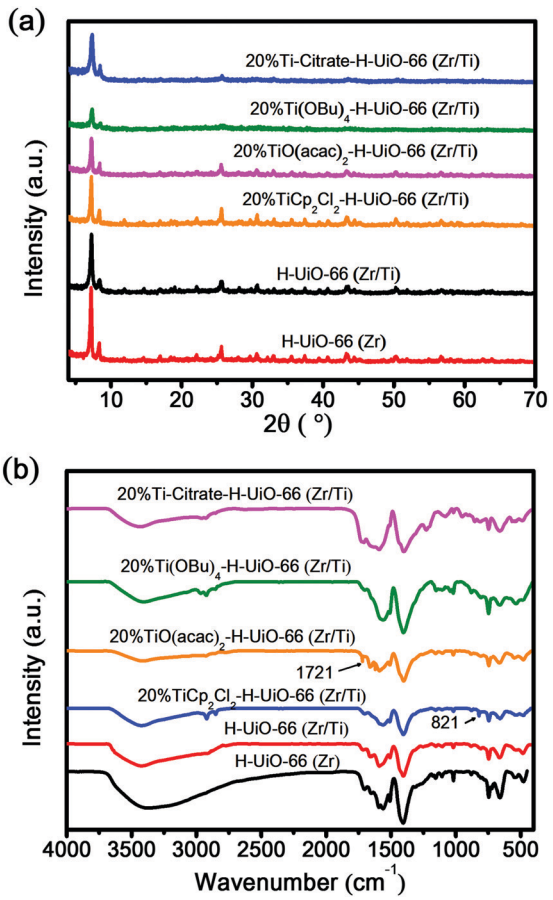

Fig. 1 (a) XRD patterns and (b) FT-IR spectra of the Ti functionalized H-UiO-66(Zr/Ti) catalysts.

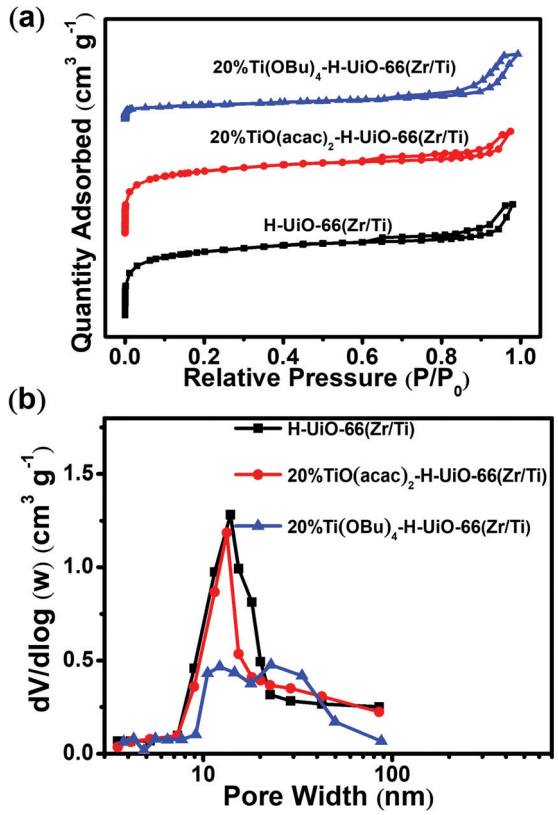

Fig. 2 (a) N_2 adsorption–desorption isotherms at 77 K and (b) mesopore size distributions of Ti functionalized H-UiO-66(Zr/Ti) prepared with different Ti sources.

sites of the H-UiO-66(Zr) framework. Additionally, the vanishing of the characteristic diffraction peak of TiO_2 crystalline phase demonstrates the amorphous state of the Ti^{IV} species. Moreover, the low relative crystallinity of 20%Ti$(OBu)_4$-H-UiO(Zr/Ti) can be ascribed to the rapid hydrolysis of $Ti(OBu)_4$ and the generation of more $Ti(OBu)_{4-x}(OH)_x$ oligomers.

The reactions between different Ti sources and H-UiO-66(Zr/Ti) were explored by FT-IR spectroscopy (Fig. 1(b)). Two strong absorption bands at approximately 1550 and 1410 cm^{-1} are associated with asymmetric stretching and symmetric stretching vibrations of O–C═O groups in the skeletons of H-UiO-66(Zr/Ti).[38] The broad bands at 3400 cm^{-1} are ascribed to hydroxyl vibration. The peak at around 821 cm^{-1} can be observed and demonstrates the stretching vibration of –CH in the Cp ring in the 20%$TiCp_2Cl_2$-H-UiO-66(Zr/Ti) sample. Consequently, a partial Cp ring can still be retained in the reaction products of $TiCp_2Cl_2$ and H-UiO-66(Zr/Ti).[39] For the 20%$TiO(acac)_2$-H-UiO-66(Zr/Ti) sample, a new peak at approximately 1721 cm^{-1} appeared, corresponding to the C═O stretching vibration of keto,[40] which resulted from the proton migration from OH to acetylacetonate groups.[41] Furthermore, $Ti(OMe)_{4-x}(acac)_x$ is formed *via* the reaction between $TiO(acac)_2$ and methanol, as reported.[42] The spectrum of 20%Ti$(OBu)_4$-H-UiO-66(Zr/Ti) shows broad bands at 450–800 cm^{-1}, which are the characteristic frequencies of Ti–O–Ti bonds.[43] However, no Ti–O–Ti bond derived from oligomers containing Ti^{IV} can be detected when using $TiCp_2Cl_2$ or $TiO(acac)_2$. Additionally, for the 20%Ti-Citrate-H-UiO-66(Zr/Ti) catalysts, the antisymmetric stretching vibrations in the range of 1663–1580 cm^{-1} can be attributed to the presence of carboxylate carbonyls, indicating the formation of free citrate ligand or monodentate Ti-Citrate.[44–47]

As shown in Fig. 2(a) and Fig. S2(a) (ESI†), the N_2 sorption isotherms of all samples at low relative pressure correspond to the existence of micropores, and those at relative pressure higher than 0.6 indicate the generation of mesopores in the framework of the catalysts. Moreover, for all samples, the hystereses are characteristic of solids consisting of nonuniform size and shape pores, because $Zn_4O(BC)_6$, as a mesopore template, can undergo decomposition or rearrangement in the *in situ* self-assembly reaction.[33,48] Some structural features of Ti functionalized H-UiO-66(Zr/Ti) catalysts are listed in Table 1 and Fig. S3 (ESI†). The specific surface area of H-UiO-66(Zr/Ti) and micropore size slightly increase to 1220 and 0.62 from the original 1108 $m^2\ g^{-1}$ and 0.60 nm, which suggests that the Ti^{IV} ions are incorporated into the secondary building unit (SBU) clusters and few Ti^{IV} species are blocking the pores. The increase in the surface area and pore size of H-UiO-66(Zr/Ti) can be ascribed to the lighter atomic weight and lower maximum coordination number of Ti^{IV} compared to those of Zr^{IV}.[35,49] However, the BET surface area of 20%TiO-$(acac)_2$-H-UiO-66(Zr/Ti) and 20%$TiCp_2Cl_2$-H-UiO-66(Zr/Ti) drops slightly, indicating that some Ti^{IV} ions can be anchored on the nodes of UiO-66(Zr/Ti). When $Ti(OBu)_4$ is selected as the Ti source, the surface area of the sample is significantly reduced. The result

Table 1 Pore features of Ti functionalized H-UiO-66(Zr/Ti) catalysts

Sample	S_{BET} ($m^2\ g^{-1}$)	S_{micro} ($m^2\ g^{-1}$)	S_{meso} ($m^2\ g^{-1}$)	Micropore size (nm)	Mesopore size (nm)
TS-1	413	270	143	0.56	29.7
Conventional UiO-66(Zr)	982	917	65	0.58	18.2
H-UiO-66(Zr) precursor	575	423	152	0.64	25.4
H-UiO-66(Zr)	1108	755	353	0.60	12.9
H-UiO-66(Zr/Ti)	1220	865	355	0.62	13.9
20%$TiCp_2Cl_2$-H-UiO-66(Zr/Ti)	1031	694	337	0.61	13.9
20%$TiO(acac)_2$-H-UiO-66(Zr/Ti)	1092	771	321	0.61	13.3
20%Ti$(OBu)_4$-H-UiO-66(Zr/Ti)	588	326	262	0.50	17.4
20%Ti-Citrate-H-UiO-66(Zr/Ti)	859	573	286	0.59	13.7

S_{BET} is the Brunauer–Emmett–Teller (BET) specific surface area. S_{micro} is the *t*-plot-specific micropore surface area calculated from the N_2 adsorption–desorption isotherm. S_{meso} is the specific mesopore surface area estimated by subtracting S_{micro} from S_{BET}. The micropore diameter represent the median pore width which was calculated by Horvath–Kavazoe method.

supports the argument that many $Ti(OBu)_{4-x}(OH)_x$ oligomers are deposited in the pores of the support. Additionally, the introduction of Ti-Citrate can cause a decrease in the catalyst surface area due to its larger molecular diameter and stability in solution. Moreover, in Fig. 2(b) and Fig. S2(b) (ESI†), the mesopore size distributions (calculated by BJH method) of 20%$TiO(acac)_2$-H-UiO-66(Zr/Ti) and 20%$TiCp_2Cl_2$-H-UiO-66(Zr/Ti) are similar to that of H-UiO-66(Zr/Ti), whereas the mesopore volume is slightly smaller than that of unmodified H-UiO-66(Zr/Ti). These results indicate that few Ti^{IV} species can be observed on the oligomers.

The chemical states and contents of the Ti and O species over the surface of samples were studied by using X-ray photoelectron spectroscopy (XPS). According to the high resolution scan spectra of Ti atoms illustrated in Fig. 3(a), the Ti $2p_{3/2}$ signal of the samples can be decomposed into two contributions at 458.1 eV and 458.9 eV, which correspond to octahedral coordinated Ti^{IV} and tetrahedral coordinated Ti^{IV}, respectively.[50] The two different contributions of Ti^{IV} of the a photoelectron signal were determined by the percentage of their areas (Table S1, ESI†). After ion exchange treatment, the Ti^{IV} cations of H-UiO-66(Zr/Ti) are distributed as 72.5% in octahedral sites and 27.5% in tetrahedral sites. Therefore, the incorporation of Ti^{IV} ions into the H-UiO-66(Zr) framework is achieved by using $TiCp_2Cl_2$ as a Ti source under solvent thermal conditions. Moreover, the contents of octahedral coordinated Ti^{IV} and tetrahedral coordinated Ti^{IV} are approximately 2.78 at% and 1.05 at% in the sample (Table S2, ESI†). When H-UiO-66(Zr/Ti) was treated by refluxing with a different Ti source, more surface tetrahedral coordinated Ti^{IV} species appeared. Besides, as shown in Table S2 (ESI†), the octahedral coordinated Ti/Zr molar ratios almost remain constant for 20%$TiCp_2Cl_2$-H-UiO-66(Zr/Ti) and 20%$TiO(acac)_2$-H-UiO-66(Zr/Ti) samples. However, the central Ti^{IV} ion of mononuclear Ti-Citrate has adopted a six-coordinated arrangement to three α-carboxyl groups derived from three citrate ligands, forming a distorted octahedral geometry.[47] There is an equilibrium of dissociation of the tetradentate and hexacoordinate Ti-Citrate complexes in PH ≈ 7 solution.[46] Furthermore, Ti-Citrate possesses excellent hydrolytic stability and less tetradentate hydrolysis products. Consequently, for the 20%Ti-Citrate-H-UiO-66(Zr/Ti) sample, the percentage of octahedral coordinated Ti^{IV} species is significantly increased as compared to that of 20%$TiO(acac)_2$-H-UiO-66(Zr/Ti). Additionally, in Fig. 3(b), the samples containing Ti^{IV} species has asymmetric O 1s signals that can be decomposed into four contributions locating at 532.65, 531.7, 530.7 and 530.1 eV. The four peaks are assigned to hydroxyl, C═O, Zr–O, and Ti–O species on the surface of the samples, respectively.[34,51,52] The existence of the Ti–O bond implies that the Ti^{IV} moieties are probably introduced into the framework or linker vacancy sites of H-UiO-66(Zr) *via* the formation of an oxo-bridge.

As shown in Fig. S4 (ESI†), the hierarchical-pore UiO-66(Zr) shows irregular spherical agglomerations instead of the layered structure of conventional UiO-66(Zr) with pure micropores. And the morphology of Ti functionalized H-UiO-66(Zr/Ti) is displayed in Fig. 4. The samples present spherical agglomerations, which are similar to that of H-UiO-66(Zr). In Fig. 4(a) and (b), the outer surface of the spheres is smooth, indicating that almost no Ti oligomer particles can be observed on the surface of 20%$TiCp_2Cl_2$-H-UiO-66(Zr/Ti) and 20%$TiO(acac)_2$-H-UiO-66(Zr/Ti). However, the surface of 20%$Ti(OBu)_4$-H-UiO-66(Zr/Ti) (Fig. 4(c)) became rough due to the rapid hydrolysis of $Ti(OBu)_4$

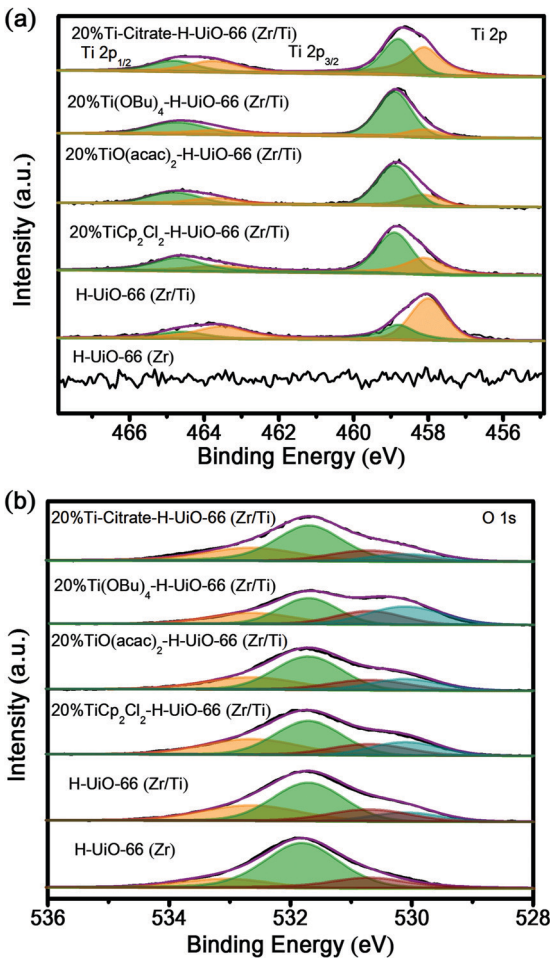

Fig. 3 (a) Ti 2p XPS spectra of the synthesized samples and (b) O 1s XPS spectra of the synthesized samples.

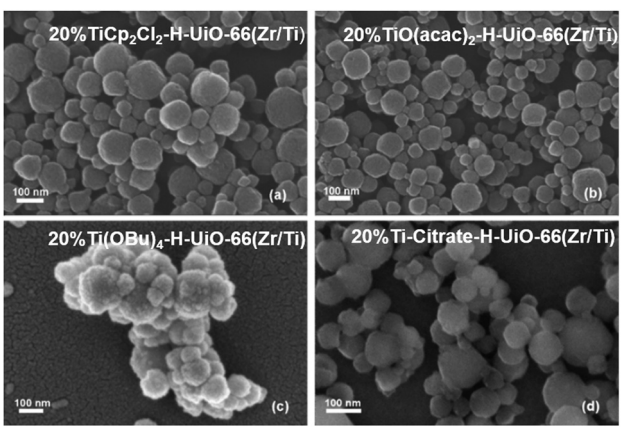

Fig. 4 SEM images of samples.

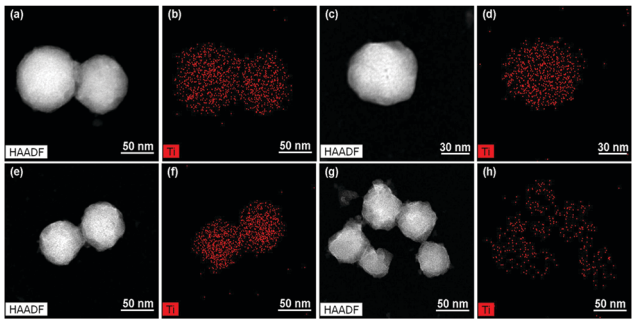

Fig. 5 (a), (c), (e), and (g) STEM-HAADF image and (b), (d), (f), (h) corresponding Ti elemental maps of 20%$TiCp_2Cl_2$-H-UiO-66(Zr/Ti), 20%$TiO(acac)_2$-H-UiO-66(Zr/Ti), 20%$Ti(OBu)_4$-H-UiO-66(Zr/Ti) and 20%Ti-Citrate-H-UiO-66(Zr/Ti).

and the generation of lots of $Ti(OBu)_{4-x}(OH)_x$ oligomers.[17] Additionally, some floccules appeared on the surface of 20%Ti-Citrate-H-UiO-66(Zr/Ti) because of the centrosymmetric oligomers transforming from the linear hydrogen bonding of the uncoordinated protonated β-carboxylic acid to the deprotonated β-carboxyl group.[46] The results were in good agreement with those from N_2 adsorption–desorption.

The STEM-HAADF and Ti elemental mappings of Ti functionalized H-UiO-66(Zr/Ti) catalysts are shown in Fig. 5. The Ti elemental mappings of 20%$TiCp_2Cl_2$-H-UiO-66(Zr/Ti) and 20%$TiO(acac)_2$-H-UiO-66(Zr/Ti) demonstrate the homogeneous distribution of Ti^{IV} species in the whole catalyst crystals. Therefore, the uniformly distributed tetradentate Ti^{IV} species can be realized by using $TiCp_2Cl_2$ or $TiO(acac)_2$ as a Ti source. In contrast, 20%$Ti(OBu)_4$-H-UiO-66(Zr/Ti) displays a slightly higher Ti content inside the particles than the surface amount of Ti, indicating that more Ti^{IV} species block the internal pores in the particles. In addition, the content of Ti species on the surface is higher than that in the inner part of the particles, which suggests that more Ti-Citrate or its oligomers were anchored on the surface of H-UiO-66(Zr/Ti) due to the larger molecular diameter.

Properties of the catalysts

A series of Ti functionalized H-UiO-66(Zr/Ti) as heterogeneous catalysts was employed for the transesterification of PA and DMC to synthesize DPC. The stabilities of the prepared catalysts were investigated by TG analysis over the temperature range of 30–800 °C under a N_2 atmosphere. As displayed in Fig. S5 (ESI†), all catalysts show a slight loss of mass upon heating at 100–200 °C due to the removal of solvent. The result indicates that the structure of all catalysts can be retained at the reaction temperature (170–190 °C). Additionally, the industrialized production of DPC is divided into two steps: the first step is transesterification to obtain DPC and methyl phenyl carbonate (MPC) by using transesterification catalysts, and the next step is disproportionation of MPC to get high purity DPC. Therefore, MPC and DPC were considered as the main products in this work. The different parameters, such as reaction time and the performance of reused catalyst, affecting the reaction were discussed.

Effect of Ti source of catalysts on transesterification

The effect of the Ti sources of catalysts on the yield of MPC and DPC in the transesterification of PA and DMC was investigated. As shown in Table 2, H-UiO-66(Zr) exhibits higher PA conversion and MPC and DPC yields than UiO-66(Zr), which may be due to the mesopores of H-UiO-66(Zr) with large-scale defects and decreased molecular diffusion resistance (as shown in Fig. S5, ESI† and Table 1).[26] Moreover, in the TG curves (as shown in Fig. S5, ESI†), the weight loss of H-UiO-66(Zr) in the 450–700 °C interval is lower than that of UiO-66(Zr), which implies more miss-linking sites that can be ascribed to the increase of structural disorder.[53] In addition, the catalyst activity can be enhanced by introducing Ti^{IV} ions, which are mainly six-coordinated with octahedron geometry, in the framework of H-UiO-66(Zr). Although six-coordinated Ti^{IV} ions show no Lewis acidity, the appearance of them can lead to the formation of more structural defects to increase the Lewis acid sites of catalysts.[53] The reason is that the ordering of the framework structure of H-UiO-66(Zr) is further decreased by different cation radiuses of Ti^{IV} and Zr^{IV} in the octahedral coordination sites of SBU.[27] More importantly, adequate hydroxyl groups can be provided by the defect sites derived from the miss links and they can be used to coordinate with the Ti^{IV} species.[35] For 20%$TiO(acac)_2$-H-UiO-66(Zr/Ti) catalyst, the conversion of PA reaches a maximum value (81.32%); the yields of DPC and MPC are 54.05% and 19.70%, respectively. Furthermore, compared to other catalysts reported in the literature, the as-synthesized

Table 2 Effect of Ti source on the activity of different catalysts

Cat	PA conversion (%)	Yield (%)			Transesterification selectivity (%)
		DPC	MPC	PhOH	
UiO-66(Zr)	35.94	16.95	13.68	5.31	85.22
H-UiO-66(Zr)	42.19	24.00	12.63	5.56	86.82
H-UiO-66(Zr/Ti)	51.24	30.14	15.93	5.17	89.91
20%$TiCp_2Cl_2$-H-UiO-66(Zr/Ti)	79.35	50.28	22.23	6.84	91.38
20%$TiO(acac)_2$-H-UiO-66(Zr/Ti)	81.32	54.05	19.70	7.57	90.69
20%$Ti(OBu)_4$-H-UiO-66(Zr/Ti)	55.87	32.04	16.08	7.75	86.13
20%Ti-Citrate-H-UiO-66(Zr/Ti)	45.48	25.85	14.39	5.24	88.48
TS-1	42.82	22.46	15.31	5.05	88.21
20%$TiO(acac)_2$-TS-1	55.93	30.58	19.55	5.80	89.63

Reaction conditions: n(DMC) = 0.44 mol, n(PA) = 0.22 mol, m(Cat) = 0.6 g, reaction temperature 170–190 °C, reaction time 7 h.

catalyst showed better catalytic activity at lower dosage. For example, Cao *et al.*[8] found that the yields of DPC and MPC are 29.1% and 41.7% for the MoO_3 catalyst in a high pressure autoclave, and the amount of catalyst reached up to 5 wt% with respect to the mass of PA. Wang *et al.*[54] disclosed that the conversion of PA was 79.21% when the dosage of TiO_2/SiO_2 was 4 wt%. We previously reported that the conversion of PA could achieve 74.65% using mesoporous amorphous TiO_2 shell-coated ZIF-8 as a catalyst, and the catalyst concentration was 3 wt%.[55] As expected, the tetra-coordinated titanium, as an active site, can interact with the C=O group of DMC and MPC to improve the catalytic activity.[11] The result can be attributed to a suitable hydrolysis rate of $TiO(acac)_2$ and tetra-coordinated Ti^{IV} products. However, no obvious improvement of the PA conversion and product yield can be observed using $Ti(OBu)_4$ as a Ti source, because $Ti(OBu)_4$ is highly sensitive to water or alcohols, and tends to generate dense precipitates fast, which can block the pores prior to reaction with the OH group of H-UiO-66(Zr/Ti).[18] Besides, Ti-Citrate cannot provide enough tetra-coordinated Ti^{IV} active sites to impel the proceeding of transesterification due to hydrolysis resistance. Additionally, TS-1 zeolite and 20%$TiO(acac)_2$-TS-1 were applied in this reaction, because the framework of TS-1 possesses tetra-coordinated Ti^{IV} species (as shown in Fig. S6, ESI†).[56] As shown in Table 2, when using TS-1 or 20%$TiO(acac)_2$-TS-1 as a catalyst, the PA conversion was lower than 60%, which can be ascribed to the fewer Ti^{IV} species and smaller surface area than those of Ti functionalized H-UiO-66(Zr/Ti) (see Table 1 and Table S3, Fig. S7, ESI†).

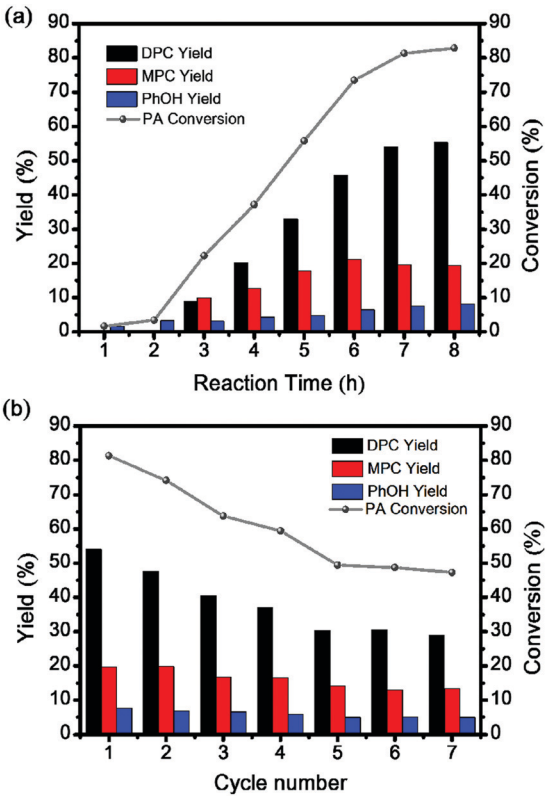

Fig. 6 (a) Effect of reaction time on the catalytic activity of 20%$TiO(acac)_2$-H-UiO-66(Zr/Ti) and (b) the reusability of 20%$TiO(acac)_2$-H-UiO-66(Zr/Ti).

Effect of reaction time of catalysts on transesterification

The reaction time has a significant influence on the activity of 20%$TiO(acac)_2$-H-UiO-66(Zr/Ti) (Fig. 6(a)). The yields of MPC and DPC increase with the extending of the reaction time from 0 to 7 h. However, when the reaction time comes to 8 h, no significant effect on the conversion of PA and yield of products is observed. When the reaction time takes longer than 6 h, the MPC yield starts to decline slightly, but the yields of DPC and phenol (PhOH) keep increasing. These results suggest that the generated MPC is disproportionated or reacted with DMC to DPC.[51,57] Moreover, the generation of PhOH by-product is mainly attributed to the rearrangement or hydrogenolysis of the transesterification products through using Lewis acid catalysts.

Reusability of 20%$TiO(acac)_2$-H-UiO-66(Zr/Ti)

Since 20%$TiO(acac)_2$-H-UiO-66(Zr/Ti) shows the highest activity of the Ti-functionalized H-UiO-66(Zr/Ti) catalysts, the reusability of it was investigated by performing the reaction under optimized conditions (n(DMC) = 0.44 mol, n(PA/DMC) = 1 : 2, m(Cat) = 0.6 g, reaction temperature 170–190 °C, reaction time 7 h). The used catalyst was centrifuged, washed with DMC several times, and dried at 100 °C after each run. Obviously, with the increase of the cycle number of catalysis, the conversion of PA and the yields of DPC and MPC show a gradual decline tendency. We conclude that tetrahedral Ti^{IV} active site leaching is the main cause of catalyst deactivation. Significantly, after 5 runs, the catalytic activity of 20%$TiO(acac)_2$-H-UiO-66(Zr/Ti) is close to that of H-UiO-66(Zr/Ti). Furthermore, the conversion of PA and the yield of products gradually stabilized with the cycle number of catalysts increasing from 5 to 7. These results can arise from the different stability of octahedral and tetrahedral coordinated Ti^{IV} ions.

The used 20%$TiO(acac)_2$-H-UiO-66(Zr/Ti) catalysts were analyzed by means of XRD and XPS. As shown in Fig. 7(a), the XRD patterns confirm that the framework structure of the 20%$TiO(acac)_2$-H-UiO-66(Zr/Ti) is unchanged, but the relative crystallinity of it is decreased after 7 runs. Besides, there is no shift of diffraction angle at $2\theta \approx 7.3^\circ$ (Fig. S8, ESI†), indicating that some octahedral Ti^{IV} ions, which are introduced by post-synthetic exchange, still remain in the metal cluster SBUs. However, there are only octahedral coordinated Ti^{IV} ions left in the catalyst after 7 consecutive cycles (Fig. 7(b)). The results support the hypothesis that the tetrahedral coordinated Ti^{IV} ions exhibit a higher catalytic activity than the octahedral coordinated Ti^{IV} ions for the transesterification process. Nevertheless, after 7 consecutive runs, the PA conversion remains at 47.25%, which is higher than that of H-UiO-66(Zr). This can be related to more miss-linking sites in the H-UiO-66(Zr/Ti) support.[37] In the catalyst support, the point defects, caused by the introduction of octahedral coordinated Ti^{IV} ions, are well retained after being used in 7 consecutive cycles and help to increase the activity of the catalyst.

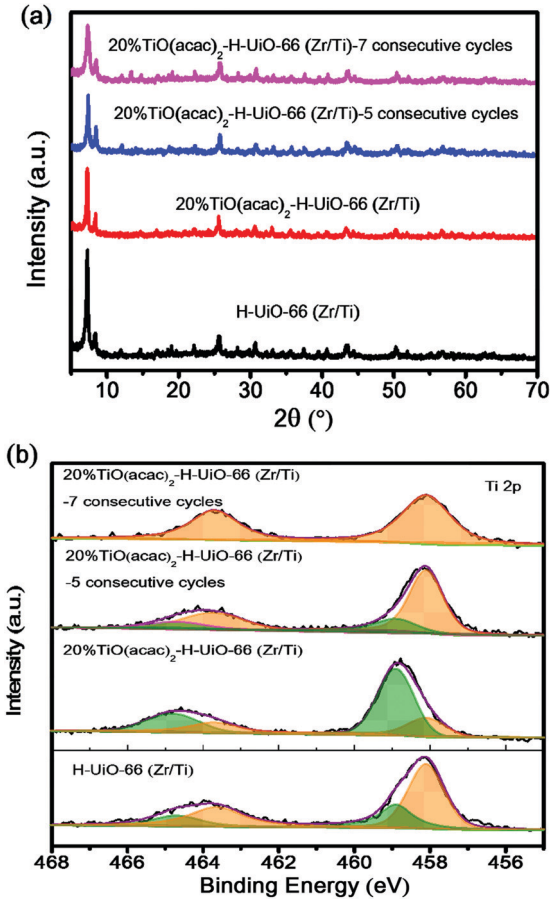

Fig. 7 (a) XRD patterns of fresh and used catalysts; (b) XPS spectra of fresh and used catalysts.

Conclusions

The hierarchical-pore UiO-66(Zr/Ti) was prepared by using acid-sensitive Zn-based metal–organic fragments as templates. And then the octahedral coordinated Ti^{IV} ions were incorporated into the framework of H-UiO-66(Zr) through ion exchange. The properties of the catalysts demonstrate that the presence of defects, including large-scale defects (mesopores) and point defects (linker vacancies or M–OH), in H-UiO-66(Zr/Ti) can enhance the catalytic activity for transesterification. Moreover, the different tetra-coordinated Ti^{IV} species were anchored on the linker vacancy sites of H-UiO-66(Zr/Ti) *via* a post-grafting method. The influence of coordination environment of Ti^{IV} ions on the catalytic activity for the transesterification of DMC with PA was also discussed. The tetra-coordinated Ti^{IV} ions are the main factor responsible for the catalytic activity during the synthesis of DPC from DMC and PA. With small catalyst consumption, 20%$TiO(acac)_2$-H-UiO-66(Zr/Ti) exhibits the best activity and selectivity, indicating that the Ti^{IV} species grafted on H-UiO-66(Zr/Ti) can have a remarkable influence on the activity of catalysts. Furthermore, after 7 consecutive runs, the yields of transesterification products can remain at 42.3% due to the Lewis acid sites of the catalyst derived from the abundant structure defects. Among the four kinds of Ti sources, $TiO(acac)_2$ exhibits excellent distribution of tetra-coordinated Ti^{IV} species on H-UiO-66(Zr/Ti), which can be attributed to the suitable hydrolytic rate and hydrolysates. However, the excess Ti–O–Ti bonds and Ti^{IV} oligomers, which are usually provided by deposited amorphous TiO_2 on catalyst supports, impede the catalytic efficiency in this reaction due to a lower utilization of Ti^{IV} active sites and a larger diffusion resistance in the pores of catalyst supports. Consequently, this study provides a promising route to overcome diffusion limitations, increase the concentration of Lewis acid sites in catalysts and effectively inhibit the generation of Ti^{IV} oligomers for catalysts containing tetra-coordinated titanium.

Conflicts of interest

The authors declare that they have no conflicts of interest.

Acknowledgements

We gratefully acknowledge the financial support from the Innovation Academy for Green Manufacture, Chinese Academy of Sciences (No. IAGM-2019-A10) and the Department of Science and Technology of Sichuan Province (No. 18ZHSF0011).

References

1 Z. Du, Y. Xiao, T. Chen and G. Wang, *Catal. Commun.*, 2008, **9**, 239–243.
2 P. Wang, S. Liu, F. Zhou, B. Yang, A. S. Alshammari and Y. Deng, *RSC Adv.*, 2015, **5**, 84621–84626.
3 W. Sun, J. Shao, Z. Xi and L. Zhao, *Can. J. Chem. Eng.*, 2017, **95**, 353–358.
4 Z. Wang, X. Yang, S. Liu and G. Wang, *J. Mol. Catal. A: Chem.*, 2016, **424**, 77–84.
5 S. Luo, T. Chen, D. Tong, Y. Zeng, Y. Lei and G. Wang, *Chin. J. Catal.*, 2007, **28**, 937–939.
6 J. Gong, X. Ma and S. Wang, *Appl. Catal., A*, 2007, **316**, 1–21.
7 S. Luo, Y. Chi, L. Sun, Q. Wang and C. Hu, *Catal. Commun.*, 2008, **9**, 2560–2564.
8 P. Cao, X. Yang, C. Tang, J. Yang, J. Yao, Y. Wang and G. Wang, *Chin. J. Catal.*, 2009, **30**, 853–855.
9 T. Murayama, T. Hayashi, R. Kanega and I. Yamanaka, *J. Phys. Chem. C*, 2012, **116**, 10607–10616.
10 G. Fan, Z. Wang, B. Zou and M. Wang, *Fuel Process. Technol.*, 2011, **92**, 1052–1055.
11 H. Yang, Z. Xiao, Y. Qu, T. Chen, Y. Chen and G. Wang, *Res. Chem. Intermed.*, 2018, **44**, 799–812.
12 K. Zhou, X. D. Xie and C. T. Chang, *Appl. Surf. Sci.*, 2017, **416**, 248–258.
13 X. Zhang, X. Ke, Z. Zheng, H. Liu and H. Zhu, *Appl. Catal., B*, 2014, **150–151**, 330–337.
14 S. Y. Chen, T. Mochizuki, Y. Abe, M. Toba and Y. Yoshimura, *Appl. Catal., B*, 2014, **148–149**, 344–356.
15 X. Ma, J. Gong, S. Wang, F. He, H. Guo, X. Yang and G. Xu, *J. Mol. Catal. A: Chem.*, 2005, **237**, 1–8.

16 R. Tang, T. Chen, Y. Chen, Y. Zhang and G. Wang, *Chin. J. Catal.*, 2014, **35**, 457–461.
17 D. Chen, L. Cao, F. Huang, P. Imperia, Y. B. Cheng and R. A. Caruso, *J. Am. Chem. Soc.*, 2010, **132**, 4438–4444.
18 R. Zhang, A. A. Elzatahry, S. S. Al-Deyab and D. Zhao, *Nano Today*, 2012, **7**, 344–366.
19 S. Wang, C. Li, Z. Xiao, T. Chen and G. Wang, *J. Mol. Catal. A: Chem.*, 2016, **420**, 26–33.
20 J. Kansedo and K. T. Lee, *Biomass Bioenergy*, 2012, **40**, 96–104.
21 C. M. Granadeiro, S. O. Ribeiro, M. Karmaoui, R. Valenca, J. C. Ribeiro, B. de Castro, L. Cunha-Silva and S. S. Balula, *Chem. Commun.*, 2015, **51**, 13818–13821.
22 V. N. Panchenko, M. M. Matrosova, J. Jeon, J. W. Jun, M. N. Timofeeva and S. H. Jhung, *J. Catal.*, 2014, **316**, 251–259.
23 A. Dhakshinamoorthy, A. Santiago-Portillo, A. M. Asiri and H. Garcia, *ChemCatChem*, 2019, **11**, 899–923.
24 M. Vandichel, J. Hajek, F. Vermoortele, M. Waroquier, D. E. D. Vosb and V. V. Speybroeck, *CrystEngComm*, 2015, **17**, 395–406.
25 L. Liu, Z. Chen, J. Wang, D. Zhang, Y. Zhu, S. Ling, K. W. Huang, Y. Belmabkhout, K. Adil, Y. Zhang, B. Slater, M. Eddaoudi and Y. Han, *Nat. Chem.*, 2019, **11**, 622–628.
26 Z. Fang, B. Bueken, D. E. D. Vos and R. A. Fischer, *Angew. Chem., Int. Ed.*, 2015, **54**, 7234–7254.
27 M. Kim, J. F. Cahill, H. Fei, K. A. Prather and S. M. Cohen, *J. Am. Chem. Soc.*, 2012, **134**, 18082–18088.
28 H. Song, J. A. You, B. Li, C. Chen, J. Huang and J. Zhang, *Chem. Eng. J.*, 2017, **327**, 406–417.
29 J. G. Santaclara, A. I. Olivos-Suarez, A. Gonzalez-Nelson, D. Osadchii, M. A. Nasalevich, M. A. van der Veen, F. Kapteijn, A. M. Sheveleva, S. L. Veber, M. V. Fedin, A. T. Murray, C. H. Hendon, A. Walsh and J. Gascon, *Chem. Mater.*, 2017, **29**, 8963–8967.
30 H. Wu, Y. S. Chua, V. Krungleviciute, M. Tyagi, P. Chen, T. Yildirim and W. Zhou, *J. Am. Chem. Soc.*, 2013, **135**, 10525–10532.
31 F. Vermoortele, B. Bueken, G. L. Bars, B. Van de Voorde, M. Vandichel, K. Houthoofd, A. Vimont, M. Daturi, M. Waroquier, V. Van Speybroeck, C. Kirschhock and D. E. D. Vos, *J. Am. Chem. Soc.*, 2013, **135**, 11465–11468.
32 L. G. Qiu, T. Xu, Z. Q. Li, W. Wang, Y. Wu, X. Jiang, X. Y. Tian and L. D. Zhang, *Angew. Chem., Int. Ed.*, 2008, **47**, 9487–9491.
33 H. Huang, J. R. Li, K. Wang, T. Han, M. Tong, L. Li, Y. Xie, Q. Yang, D. Liu and C. Zhong, *Nat. Commun.*, 2015, **6**, 8847.
34 A. Wang, Y. Zhou, Z. Wang, M. Chen, L. Sun and X. Liu, *RSC Adv.*, 2016, **6**, 3671–3679.
35 H. G. T. Nguyen, L. Mao, A. W. Peters, C. O. Audu, Z. J. Brown, O. K. Farha, J. T. Hupp and S. B. T. Nguyen, *Catal. Sci. Technol.*, 2015, **5**, 44444451.
36 A. S. Portillo, H. G. Baldoví, M. T. G. Fernandez, S. Navalón, P. Atienzar, B. Ferrer, M. Alvaro, H. Garcia and Z. Li, *J. Phys. Chem. C*, 2017, **121**, 7015–7024.
37 A. Santiago-Portillo, S. Navalón, M. Álvaro and H. García, *J. Catal.*, 2018, **365**, 450–463.
38 X. Min, X. Wu, P. Shao, Z. Ren, L. Ding and X. Luo, *Chem. Eng. J.*, 2019, **358**, 321–330.
39 J. H. Toney and T. J. Marks, *J. Am. Chem. Soc.*, 1985, **107**, 947–953.
40 C. Shen and L. L. Shaw, *J. Sol-Gel Sci. Technol.*, 2010, **53**, 571–577.
41 I. O. Acik, J. Madarász, M. Krunks, K. Tánsuaadu, D. Janke, G. Pokol and L. Niinistö, *J. Therm. Anal. Calorim.*, 2007, **88**, 557–563.
42 C. T. Chen and Y. S. Munot, *J. Org. Chem.*, 2005, **70**, 8625–8627.
43 X. Zeng, L. Huang, C. Wang, J. Wang, J. Li and X. Luo, *ACS Appl. Mater. Interfaces*, 2016, **8**, 20274–20282.
44 M. Dakanali, E. T. Kefalas, C. P. Raptopoulou, A. Terzis, G. Voyiatzis, I. Kyrikou, T. Mavromoustakos and A. Salifoglou, *Inorg. Chem.*, 2003, **42**, 4632–4639.
45 J. M. Collins, R. Uppal, C. D. Incarvito and A. M. Valentine, *Inorg. Chem.*, 2004, **44**, 3431–3440.
46 Y. F. Deng, Z. H. Zhou and H. L. Wan, *Inorg. Chem.*, 2004, **43**, 6266–6273.
47 E. T. Kefalas, P. Panagiotidis, C. P. Raptopoulou, A. Terzis, T. Mavromoustakos and A. Salifoglou, *Inorg. Chem.*, 2005, **44**, 2596–2605.
48 G. Leofanti, M. Padovan, G. Tozzola and B. Venturelli, *Catal. Today*, 1998, **41**, 207–219.
49 U. Schubert, *J. Mater. Chem.*, 2005, **15**, 3701–3715.
50 M. A. Arillo, M. L. López, C. Pico, M. L. Veiga, A. Jimenez-Lopez and E. Rodíguez-Castellon, *J. Alloys Compd.*, 2001, **317–318**, 160–163.
51 C. Tao, X. Zou, K. Du, G. Zhou, H. Yan, X. Yuan and L. Zhang, *J. Alloys Compd.*, 2018, **747**, 43–49.
52 Z. Niu, Q. Guan, Y. Shi, Y. Chen, Q. Chen, Z. Kong, P. Ning, S. Tian and R. Miao, *New J. Chem.*, 2018, **42**, 19764–19770.
53 Y. Han, M. Liu, K. Li, Q. Sun, W. Zhang, C. Song, G. Zhong, Z. C. Zhang and X. Guo, *Inorg. Chem. Front.*, 2017, **4**, 1870–1880.
54 L. Wang, X. Yang, L. Liu and G. Wang, *Petrochem. Technol.*, 2012, **41**, 770–777.
55 B. Jia, P. Cao, H. Zhang and G. Wang, *J. Mater. Sci.*, 2019, **54**, 9466–9477.
56 C. Pang, J. Xiong, G. Li and C. Hu, *J. Catal.*, 2018, **366**, 37–49.
57 X. Yin, Y. Zeng, J. Yao, Z. Du, H. Zhang, T. Sun and G. Wang, *Chem. Eng. Sci.*, 2019, **199**, 478–485.